JET-P(96)24

The Scaling of the Giant ELM Frequency

W Kerner, O Pogutse.

JET Joint Undertaking, Abingdon, Oxfordshire, OX14 3EA, UK.

Preprint of a paper to be submitted for publication in
Nuclear Fusion (letters)

July 1996

ABSTRACT

A dimensionally correct expression for the scaling of the giant ELM frequency based on the MHD interchange instability is presented. Tokamak experiments reveal that ELM events can happen well below the ideal MHD threshold. The physical model is extended in two ways, namely to include geometrical effects and dissipative terms. It is shown that both effects can play an important role in the explanation of the ELM physics.

1. INTRODUCTION

In high performance tokamaks the core plasma and the edge plasma are tightly connected and determine the physics of the tokamak confinement. At first we outline schematically our understanding of this interaction in connection with ELM activities. The tokamak edge plasma includes a part of the core plasma and a scrape-off-layer part about a few Larmor radii inside and outside of the separatrix. These parts have quite different topology with closed and open magnetic field lines, respectively. Due to MHD activity these two areas can interact. Therefore, the edge plasma plays a critical role in the behaviour of the entire plasma.

At the initial stage of the tokamak discharge resistive interchange and drift instabilities take place at the cold plasma boundary causing large turbulent transport there. This turbulence can be transferred into the centre of the plasma by a pumping mechanism or by an extended radial mode structure [1], [2]. This plasma state corresponds to L-confinement. With increasing edge temperature the dissipative instabilities become weaker, the transport coefficients are thereby reduced and the gradient in the profiles at the boundary is increased. The profile of the pressure (along with temperature and density) becomes increasingly more step-like. For such steep gradients the Larmor radius stabilisation or the shear flow stabilisation of the interchange and drift modes take place [3], [4]. Consequently the turbulence is suppressed and the H-mode is set up. Moreover, the development of a step-like pressure profile in the H-mode will lead to unstable MHD surface modes, which can explain the essential properties of the ELM phenomenon [5].

The ELMs are MHD-type perturbations [6] with widely varying amplitudes and repetition rates. Following the classification of work [7] we refer to the 'giant ELM', when the core plasma inside the separatrix is close to the ideal MHD ballooning limit. In this case the ELM repetition rate is proportional to the applied heating power. From MHD studies of ELMs in JET it has become clear that crucial elements are a local steepening of the edge pressure and current density profiles during the H-mode phase.

It was shown in the papers [8],[9] that the MHD instability can appear at first near the X-point giving rise to a precursor event. This instability removes plasma from this region and

destroys the separatrix. Both these processes lead to a strong interaction with the end plates and the wall of the chamber. Next, the region near the X-point is filled by cold, high - Z_{eff} plasma with low conductivity. This "new" plasma then acts as a poorly conducting target plate for the main plasma just inside the separatrix, which unfreezes the plasma from the field and permits the release of substantial internal thermal energy through the MHD interchange surface modes [8],[10]. This explains why the ELM can appear below the ideal MHD interchange threshold. Impurities can play the same role for triggering this instability [11]. These surface modes have a significant radial extent, which explains the macroscopic character of the ELM. Finally, this model yields an estimate for the ELM repetition time and explains thereby the occurrence of three different time scales during a giant ELM. These are the initial rise, where the first stage is given by the precursor event, which is followed by a fast MHD burst , i.e. the second stage is the giant ELM itself, removing a plasma layer from the periphery. The third phase is determined by the diffusive refilling of the expelled layer.

In the following sections we briefly explain our previous results concerning the influence of the X-point geometry on the plasma stability and then discuss the role of the dissipation in lowering the beta threshold for the interchange instability.

2. ELMS AS INTERCHANGE MODES

The physical effects which occur as a consequence of the non-linear development of the interchange modes [8] are now discussed. We first summarise the essence of our physical picture of the processes involved.

According to the previously mentioned theory the development of the ELM starts near the X-point in form of a precursor [8], [10]. Due to the destruction of the magnetic topology in the vicinity of the X-point impurities cold plasma can flow locally into the inner hot region and can trigger the main instability just inside the separatrix. This stage constitutes the giant ELM event. After this short MHD instability the slow process of the refilling of the removed plasma layer by hot plasma from the core into the periphery sets in.

Thus this picture includes the following key elements: 1) the condition for the onset of the precursor event. This is the necessary condition for the appearance of the giant ELM (this condition has been derived in [8] and more accurately in [10]); 2) the estimate of the concentration of impurities and cold plasma near the X-point being sufficient to trigger the giant ELM presented in the Appendix and 3) the estimate of the energy loss due to the non-linear stage of the interchange instability. Eventually, the combination of these processes defines the giant ELM frequency scaling.

From the linear stability theory the main parameters of the precursor perturbation are found, which allows us to derive estimates for the non-linear evolution.

This instability starts if the pressure gradient at the separatrix exceeds the critical value [8], [10]:

$$\frac{q^2 4\pi p_0}{B_0^2} > \frac{(\Delta x)_0 R q^2}{L_{\|}^2} \propto \frac{(\Delta x)_0}{R}, \tag{2.1}$$

where q is the safety factor near the separatrix, B_0 is the toroidal magnetic field, p_0 and $(\Delta x)_0$ denote the plasma pressure and the pressure gradient length at the separatrix in the mid plane, R is the major radius and $L_{\|}$ the connection length. We assume that $L_{\|} \propto qR$ (this relation contains possibly a large numerical factor). The expression (2.1) is the simplest dimensional estimate for the critical pressure if we take into account only the vicinity of the X-point. More accurate calculations introduce in the right hand side an additional dimensionless function depending on shear, ellipticity and triangularity [12]. This extended analysis allows to derive the dependence of the ELM frequency on these parameters. However, for the correct separatrix geometry including the plasma regions both inside and outside the separatrix the corresponding stability calculation has yet not been done. Therefore, we will use the estimate (2.1) as a first approximation.

The precursor perturbations near the X-point define flux tubes with width $(\Delta X)_X$ and a long tail according to the eigenfunction structure [8]. The relation between the length $(\Delta X)_X$ and the pressure gradient length in the mid plane $(\Delta X)_0$ is given by:

$$(\Delta x)_X \approx ((\Delta x)_0 y_0)^{1/2}, \tag{2.2}$$

where $y_0 \sim b$ denotes the vertical semi axis of the elliptical plasma cross section. During the MHD phase a plasma tube with a radius given by (2.2) near the X-point is removed and dumped onto the target plates. The energy which is lost during this event is in the order of

$$\Delta W_X \approx \pi \left[(\Delta x)_X\right]^2 P_{edge} \cdot 2\pi R, \tag{2.3}$$

where P_{edge} is the plasma pressure at the separatrix. From (2.3) we can estimate the relative energy loss:

$$\delta_X = \frac{\Delta W_X}{W} \approx \frac{\pi (\Delta x)_X^2}{\pi ab} \frac{P_{0edge}}{\overline{P_0}}. \tag{2.4}$$

Here $W = 2\pi^2 abR\overline{P_0}$ is the total energy content, when the area of the plasma cross section is approximately πab and $\overline{P_0}$ is the average plasma pressure.

If we choose $(\Delta x)_X \sim 15$cm, a ~ 100cm, b ~ 200cm and $P_{0edge}/P_0 \sim 0.2$ than $\delta_X \sim 0.2$ %. This value δ_X is too small to account for the energy lost during a giant ELM, i.e. the interchange instability near the X-point can only constitute a precursor event. This can explain some experimental results stating that ELMs initially appear preferentially near the X-point. When the perturbations near the X-point become sufficiently large they can trigger the interchange instability of the main plasma. In the Appendix it is shown that the critical beta for the core plasma is lowered due to the occurrence of cold plasma with low conductivity in the region near the X-point (or limiter).

The core plasma interchange instabilities can release much more energy than those localised near the separatrix . They are macroscopic and consequently the separatrix effects do not play an important role. Therefore, we can consider the region inside the separatrix with a radial width of the order of a/nq (see below) in the usual quasi-cylindrical approximation. Then the perturbations at the plasma surface comprise a plasma tube with a width in the order of a/m (the most unstable modes have a poloidal mode number m ~ nq) and with a length qR. These perturbations have the effective radial width $\Delta a \approx a/(nq)$ and a global poloidal extent. A plasma layer of width Δa near the boundary is removed during the non-linear stage of the global instability. This gives the following estimate for the lost energy:

$$\Delta W \approx \pi ab \frac{P_{0edge}}{(nq)} \cdot 2\pi R. \tag{2.5}$$

From (2.5) we can estimate the relative energy lost by means of the global interchange instability:

$$\delta = \frac{\Delta W}{W} \approx \frac{P_{0edge}}{(nq)\overline{P_0}}. \tag{2.6}$$

For n ~ 1, q ~ 5 and $P_{0edge}/\overline{P_0} \sim 0.2$ this yields $\delta \sim 4\%$.

The time necessary to restore the lost energy (2.5) due to heating is:

$$\frac{1}{\tau} = \frac{\mathrm{P}}{\Delta W}, \tag{2.7}$$

where P is the heating power. The result (2.7) defines the ELM repetition frequency. Combining (2.5) and (2.7) we find:

$$\tau \approx \frac{\pi ab P_{0edge}}{(nq)\mathrm{P}} \approx \frac{1}{nq} \frac{W}{\mathrm{P}} \frac{P_{0edge}}{\overline{P_0}}, \tag{2.8}$$

where W is again the total energy content. As an approximate estimate of (2.8) we can write:

$$\tau \approx \frac{1}{nq}\tau_E \frac{P_{0edge}}{\overline{P}_0}, \tag{2.9}$$

where $\tau_E \approx W/P$ is the energy confinement time. For n ~ 1, q ~ 5 and $P_{0edge}/\overline{P}_0 \sim 0.2$ one has $\tau \approx 4 \cdot 10^{-2}\tau_E \sim 4$ - 20 msec.

We can rewrite the formula (2.8) in a more physical way by estimating the edge plasma pressure from the stability condition (2.1):

$$f = \frac{1}{\tau} \propto nq\frac{P}{W} \propto \frac{qP}{I^2(\Delta x)_0^{1/2}}, \tag{2.10}$$

where $(\Delta x)_0$ is the pressure gradient length scale at the separatrix in the mid-plane. From this result it follows that the ELM frequency scales linearly with the applied heating power, but stronger than inversely with the total current. The specific form of the pressure gradient contributes through the width $(\Delta x)_0$. However, this dependence is weak.

The theoretical scaling (2.10) for the giant ELM frequency is the base for comparison with the experimental results. The experimentally observed ELM frequencies are presented in Figs. 1 and 2. In Fig. 1. The theoretical predicted linear dependence of the ELM frequency on the heating power can be recognised clearly. In the relations (2.7) and (2.10) P denotes the heating power, i.e. the power lost by radiation need to be subtracted from the total heating power. It is found that these particular experimental results can be fitted well by subtraction of 1.5 MW as losses from the total heating power. Afterwards we use this result to fit the current dependence of the scaling. This result is plotted in Fig. 2. It is seen that the current dependence of the experimental data is weaker than $1/I^2$ which follows from (2.10) when q ~ B_0/I is constant in accordance with the experimental condition. The fact that the scaling is weaker than $1/I^2$ can be explained by the $(\Delta x)_0$ dependence on the current. If we suppose that $(\Delta x)_0$ scales as the poloidal Larmor radius then $(\Delta x)_0 \propto 1/I$ and we obtain approximately $f \propto 1/I^{1.5}$. Therefore, it is concluded that the experimental results should have a current dependence between $1/I^{1.5}$ and $1/I^2$.

For the JET results the following dimensional expression fits the experimental data for the giant ELM frequency:

$$f_{Hz} = \frac{8.9}{I_{MA}^{1.84}}(P_{MW} - P_{radMW}). \tag{2.11}$$

This scaling is shown in Fig. 2. For these particular experiments the radiation power loss is found as $P_{radMW} = 1.5MW$. The value 8.9 in (2.11) is constant only for the simple model

used here. For a more realistic tokamak geometry it is a function of ellipticity and triangularity and q as noted earlier.

The key idea of the proposed scaling for the ELM frequency is the use of the stability condition for the interchange modes as the criterion of the ELM appearance. It is, however, well known that the plasma stability depends on the shear, ellipticity and triangularity of the plasma configuration. If we take into account this dependence we obtain instead of (2.1) the following criteria:

$$\frac{q^2 4\pi p_0}{B_0^2} > \frac{(\Delta x)_0}{R} \cdot F(S,K,\delta), \tag{2.12}$$

where $F(S,K,\delta)$ is a dimensionless function , which depends on the shear S, ellipticity K and triangularity δ. It can be approximated (for S > 1) as [12], [14]:

$$F(S,K,\delta) \propto S\frac{(4K+1)}{10}. \tag{2.13}$$

The dependence on the triangularity is rather weak in the case of large shear and it is not completely known analytically. Eventually the expression for the frequency (2.10) becomes:

$$f = \frac{1}{\tau} \propto nq\frac{P}{W} \propto \frac{qP}{I^2(\Delta x)_0^{1/2}F(S,K,\delta)}, \tag{2.14}$$

which yields a decreasing of the ELM frequency with increasing shear and ellipticity. Analogously the coefficient in the expression (2.11) in front of the right hand side equals to 8.9 only for the particular value of S and K. Really it is a function of the shear and ellipticity as in (2.14).

3. CONCLUSIONS.

The existence of a separatrix changes the condition for the onset of the interchange MHD instability in a tokamak plasma. In a plasma with separatrix the edge perturbations are localised mainly near the X-point and the threshold beta for these perturbations can be lower than the beta limit for the internal perturbations. The resulting precursor perturbations remove only a small fraction of the total stored energy and mainly destroy the magnetic field topology at the separatrix near the X-point leading to an interaction with the end plates or the wall of the chamber. The interaction with the end plates or the wall leads to an influx of cold and high-Z_{eff} plasma into the X-point region. This cold plasma with low conductivity acts like an effective

target plate for a plasma layer of width $\Delta a \approx a / (nq)$ inside the separatrix. It destabilises the interchange modes of the main plasma.

This scenario allows to estimate the frequency of ELMs and its dependence on the plasma current and the heating power. The entire process includes three stages: 1) onset of the interchange instability near the X-point and influx of cold high-Z_{eff} plasma into this local region; 2) trigger of the major interchange instability due to unfreezing of the plasma from the magnetic field and 3) refilling of the removed plasma inside the separatrix by hot plasma from the centre on the (anomalous) diffusion time scale.

APPENDIX

The Instabilities near the Plasma Edge due to Local Resistivity

The influence of the divertor geometry with an X-point on the ideal interchange instability has been considered in [8], [10]. These results have been widely used in the previous sections. Here the non-trivial influence of the resistivity on the interchange modes is discussed. For this purpose the ballooning equation in a simplified quasi-cylindrical geometry (see Fig. 3) is applied. It is, however, emphasised that the toroidal divertor geometry is indeed addressed. As explained above, after the influx of impurities through the X-point resulting in a cold, high-Z_{eff} plasma in this region, the separatrix effects can be neglected in first approximation. Consequently, this region resembles a plasma near the toroidal limiter. The ballooning equation which includes the main dissipative term, namely the resistivity, is well known [13]:

$$\frac{d}{d\theta}P(\theta)\frac{d}{d\theta}\phi'-U(\theta)\phi'=0\,, \tag{A1}$$

where

$$P(\theta)=\frac{1+S^2(\theta-\theta_0)^2}{1+\dfrac{\omega_M(\theta)}{\Gamma}(1+S^2(\theta-\theta_0)^2)} \tag{A2}$$

and

$$U(\theta)=\beta^*\{\Gamma^2(1+S^2(\theta-\theta_0)^2)+(\cos\theta+S(\theta-\theta_0)\sin\theta)\}\,. \tag{A3}$$

Only one new effect is included here by taking into account an explicit dependence of the resistivity on the poloidal angle θ, i.e. the $\omega_M(\theta)$ term in the denominator of the expression (A2). This unusual dependence is natural for the limiter and divertor geometry and has direct experimental support by the observed radiation near the X-point [15].

In (A1) - (A3) θ is the ballooning co-ordinate [13] $(-\infty<\theta<\infty)$. The quantities $k_\vartheta=nq/r$ (where q is the safety factor) and $k_\perp^2=k_\theta^2(1+S^2(\theta-\theta_0)^2)$ (where $S=rq'/q$ is the shear of the magnetic field lines) denote the poloidal and transverse wave numbers respectively. All dimensional variables are normalised to the ideal MHD growth rate $\omega_g=(p_0/n_0Mx_0R)^{1/2}$, where p_0 is the plasma pressure, n_0 the density, M the ion mass, $x_0=-(1/p_0\cdot dp_0/dx)^{-1}$ the characteristic pressure gradient length and R the major radius of tokamak. radius. $\Gamma=\gamma/\sqrt{2}\omega_g$ is the dimensionless growth rate, $\beta^*=2\omega_g^2q^2R^2/C_A^2$ the normalised beta with C_A the Alfven velocity. The term

$$\omega_M(\theta) = \frac{c^2}{4\pi\sigma(\theta)\omega_g} k_\theta^2, \tag{A.4}$$

characterises the influence of the volume Spitzer conductivity $\sigma(\theta)$. We choose for (A.4) the following model expression, which describes the localisation of the dissipation near the toroidal limiter, placed at $\theta = -\pi/2$ (or near the X-point at the bottom of the chamber):

$$\omega_M(\theta) = \omega_{M0} \cdot \exp(-\alpha \cos(\theta - \pi/2)) / \exp(\alpha), \tag{A.5}$$

where ω_{M0} - characterises the value of the resistivity in the cold region and the parameter α characterises the spread in the poloidal angle $\Delta\omega \sim (2/\alpha)^{1/2}$ where the dissipation is effective (see Figs. 3 and 6).

For qualitative conclusions it is convenient to rewrite equation (A.1) in Schroedinger form eliminating the first derivative by the substitution:

$$\phi'(\theta) = u(\theta) \cdot (P(\theta))^{-1/2}. \tag{A.6}$$

Then the equation for the new function u(θ) has the form:

$$\frac{d^2}{d\theta^2} u - V(\theta) u = 0, \tag{A.7}$$

where the 'potential' given by:

$$V(\theta) = \frac{1}{4}\left(\frac{d}{d\theta} \ln P(\theta)\right)^2 + \frac{1}{2}\frac{d^2}{d\theta^2} \ln P(\theta) + U(\theta)/P(\theta). \tag{A.8}$$

The main effect of the conductivity, which is in this case non-homogeneous along the field lines, is given by the second derivative in the expression (A.8). Figs. 4 and Fig. 5 display the shape of the 'potential' for the homogeneous (Fig. 4) and inhomogeneous, localised (Fig. 5) conductivity. In spite of the very small value of the resistivity $\omega_{M0} \sim 10^{-3}$ the consequences are quite dramatic. This effect gives a very weak dependence of the instability growth rate on the parameter 'α', which characterises the poloidal localisation (Fig. 6), i.e. any local perturbation of the conductivity in the poloidal direction plays practically the same role as the much stronger perturbation of the conductivity in the circular region near the plasma boundary (Fig. 5). The resistivity near the limiter or the X-point has the effect to decrease the beta threshold for the interchange modes (see Fig. 7). It follows that the localisation of cold plasma in the poloidal direction in conjunction with a local conductivity (α= 15, $\Delta\omega \sim \pi/5 \sim 35^0$) in the order $\omega_{M0} \sim 4 \cdot 10^{-3}$ decreases the beta limit for the interchange instability by 20%.

The previous condition can be expressed through the plasma parameters:

$$nq \approx \left[10^3 \cdot \omega_{M0} \frac{(T_{ieV}^{edge} / T_{eeV}^{loc})^{1/2}}{(x_{0cm} R_M)^{1/2}} \right]^{1/2} T_{eeV}^{loc} a_M , \qquad (A.9)$$

i.e. for $\omega_{M0} \sim 4 \cdot 10^{-3}$, $a_M \sim 1m$, $R_M \sim 3m$, $T_{ev}^{loc} \approx 30eV$, $T_{ieV}^{edge} \sim 10^3 eV$ and q ~ 5 the most unstable modes have a toroidal wave number of about n ~ 5.

The real effect can be much stronger. For a realistic geometry with an X-point the magnetic field lines extend over a very long distance. This increases the influence of the local conductivity there. This effect will even be more pronounced in a realistic tokamak geometry with a magnetic well, since the local conductivity does cancel the stabilising effect of the magnetic well. Consequently, the curves on the Fig. 7 have to decrease even faster and the numerical factor in the expression has to become considerably smaller.

REFERENCES.

1. B.B.Kadomtsev, Plasma Phys. and Cont. Fussion, 34 (1992) p.1931.
2. F.Romanelli, F.Zonca, Phys. Fluids B5 (1993) p. 4081.
3. J.G.Cordey, W.Kerner and O.Pogutse, Plasma Phys. Control. Fusion 37 (1995) p. 773-785
4. A.B.Hassam, Phys. Fluids B4 (1992) p. 485.
5. The H-mode ASDEX, ASDEX Team, Nucl. Fusion 29 (1989) p. 1959.
6. W.Kerner et al., Bull. Am. Phys. Soc. 36 (1991) 2R13, p. 2310.
7. H.J.Doyle et al 1991 Proc. 18th European Conf. on Control. Fusion and Plasma Physics (Berlin 1991) vol 1 (Vienna: IAEA) p. 285.
8. O.Pogutse, J.G.Cordey, W.Kerner and B. Schunke, Proc. 22nd EPS Conf. on Controlled Fusion and Plasma Physics (Bournemouth, 1995), vol III p. 277.
9. W.Kerner and O.Pogutse, in proceedings of 21s EPS conference Controlled Fusion and Plasma Physics, Montpellier, France, 1994, vol II p.882 .
10. W.Kerner, O.Pogutse, R.Van der Linden and B.Schunke, to be published.
11. H.J.deBlank, M.F.F.Nave, W.Kerner and G.T.A.Huysmans, Resistive Ballooning Analysis for Edge Localised Modes in JET Discharge, JET-P(93)23.
12. O.Pogutse and E.Yurchenko, Review of Plasma Physics, Consult Bureau, New York - London, vol. III p. 277.
13. J.Connor, R.Hastie and B.Taylor, Proc. R. Soc. (London), Ser. A 365 (1979) 1.
14. P.Smeulders, private communication.
15. R.Reichle at al., Proc. 22nd EPS Conf. on Controlled Fusion and Plasma Physics (Bournemouth, 1995), Contributed Paper, Part III, p. III-085.

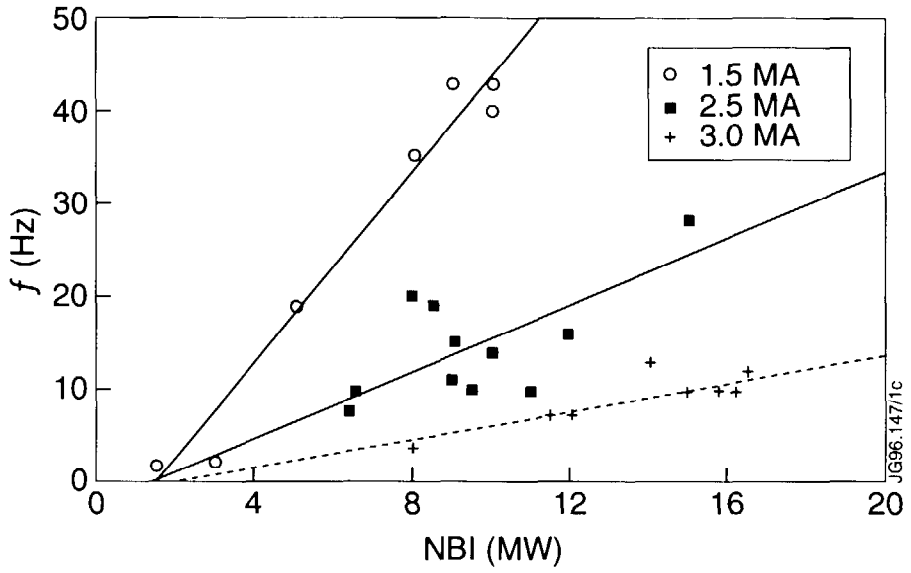

Fig. 1. The dependence of the ELM frequency on the heating power for different currents.

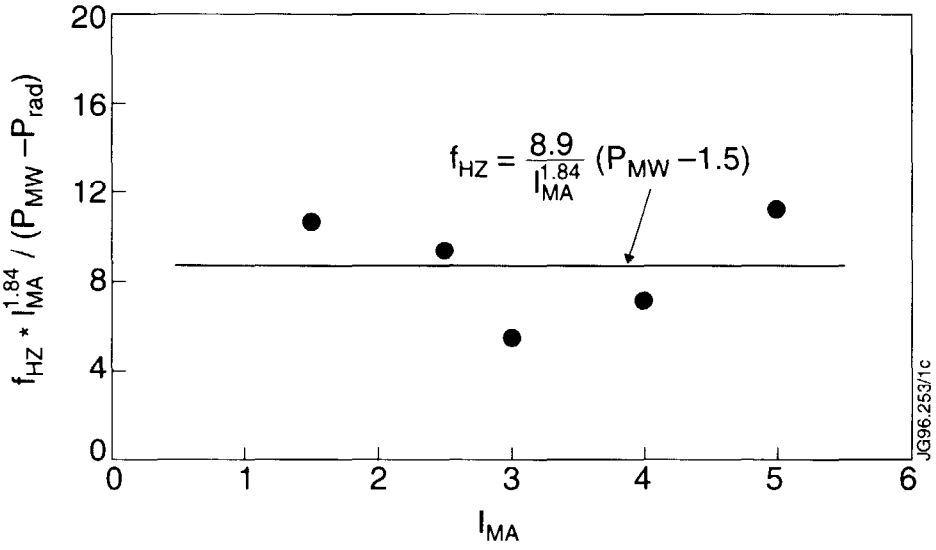

Fig. 2 The dependence of the ELM's scaling on the current.

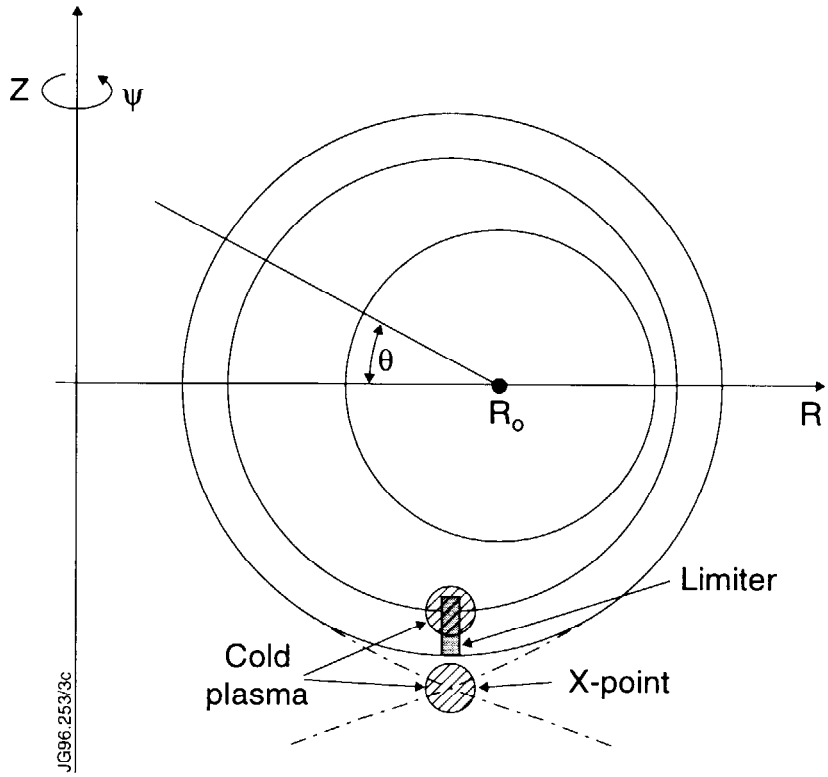

Fig. 3 The geometry of the discharge including a local cold plasma region.

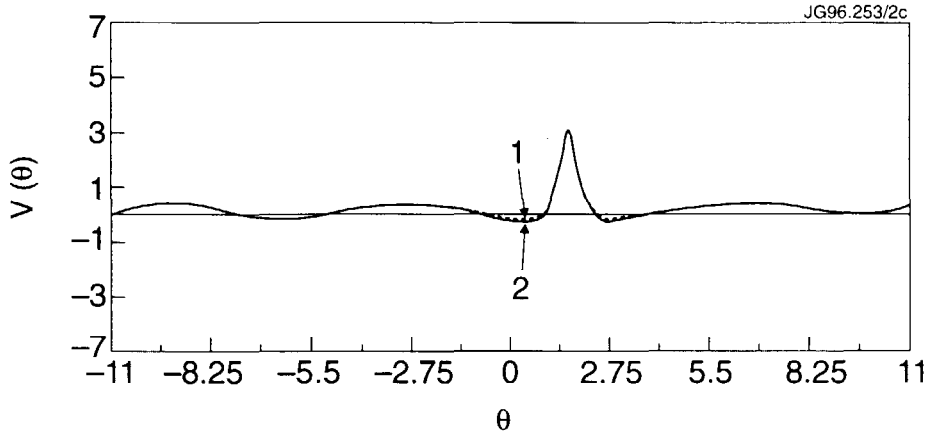

Fig. 4 The dependence of the 'potential' V(θ) of the differential equation (A.7) for the ideal case (1) and for the homogeneous resistivity (2), i.e. $\alpha = 0$, with $\omega_{M0} = 10^{-3}$ and $\beta^* = 1$, $\theta_0 = \pi/2$, $\Gamma = 0.1$, $S = 2$.

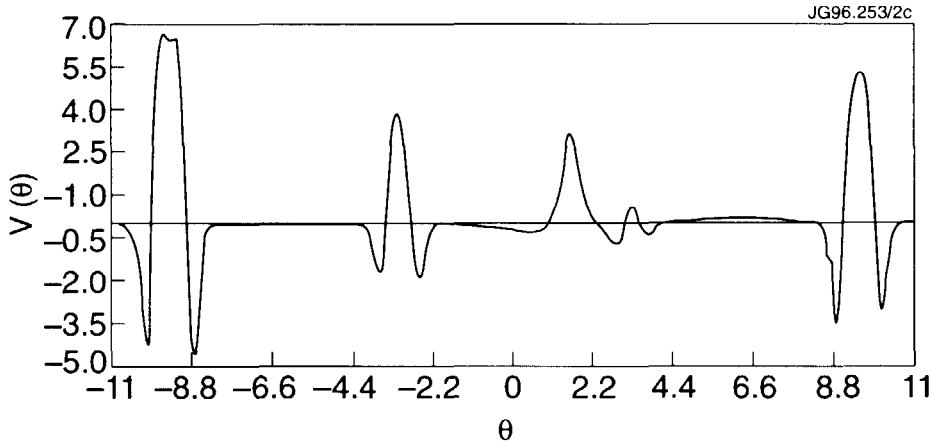

Fig. 5 The dependence of the 'potential' V(θ) for the case of an inhomogeneous ($\alpha = 15$), localised resistivity with $\omega_{M0} = 10^{-3}$, and $\beta^* = 1$, $\theta_0 = \pi/2$, $\Gamma = 0.1$, $S = 2$.

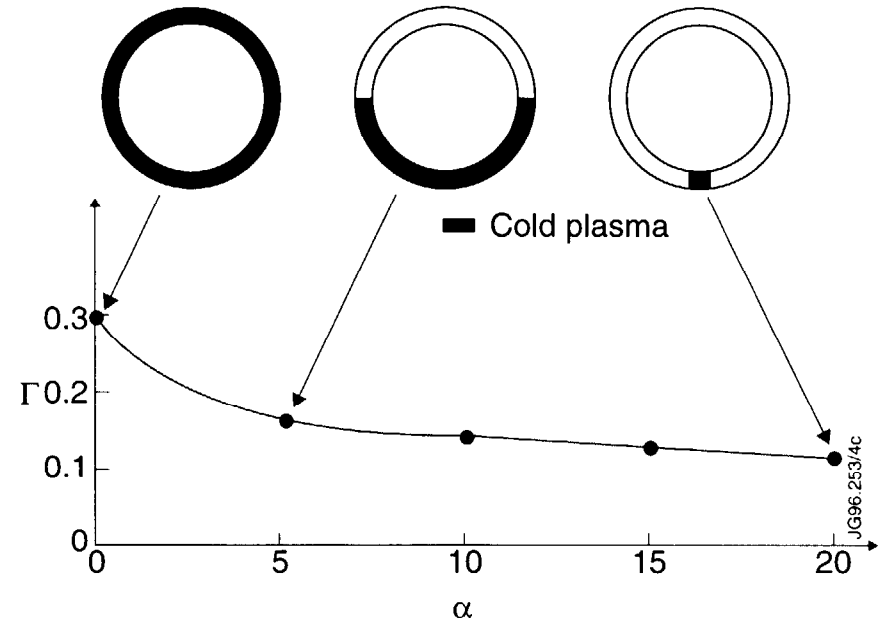

Fig. 6 The dependence of the normalised growth rate Γ on the localisation of the resistivity .

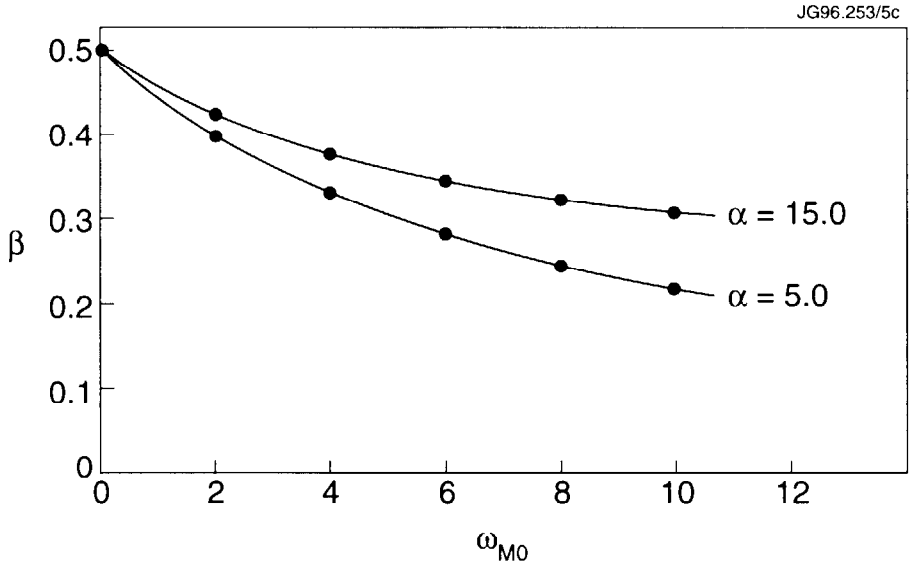

Fig. 7 The decrease of the threshold beta due to local resistivity.